Transplantation of iPSC-derived TM cells rescues glaucoma phenotypes in vivo

Wei Zhu[a,b], Oliver W. Gramlich[a], Lauren Laboissonniere[c], Ankur Jain[d], Val C. Sheffield[a,d,e], Jeffrey M. Trimarchi[c], Budd A. Tucker[a], and Markus H. Kuehn[a,b,1]

[a]Department of Ophthalmology and Visual Sciences, University of Iowa, Iowa City, IA 52242; [b]Center for the Prevention and Treatment of Visual Loss, Iowa City Veterans Affairs Medical Center, Iowa City, IA 52242; [c]Department of Genetics, Development, and Cell Biology, Iowa State University, Ames, IA 50011; [d]Department of Pediatrics, University of Iowa, Iowa City, IA 52242; and [e]Howard Hughes Medical Institute, University of Iowa College of Medicine, Iowa City, IA 52242

Edited by David J. Calkins, Vanderbilt University Medical Center, Nashville, TN, and accepted by Editorial Board Member Jeremy Nathans May 4, 2016 (received for review March 17, 2016)

Glaucoma is a common cause of vision loss or blindness and reduction of intraocular pressure (IOP) has been proven beneficial in a large fraction of glaucoma patients. The IOP is maintained by the trabecular meshwork (TM) and the elevation of IOP in open-angle glaucoma is associated with dysfunction and loss of the postmitotic cells residing within this tissue. To determine if IOP control can be maintained by replacing lost TM cells, we transplanted TM-like cells derived from induced pluripotent stem cells into the anterior chamber of a transgenic mouse model of glaucoma. Transplantation led to significantly reduced IOP and improved aqueous humor outflow facility, which was sustained for at least 9 wk. The ability to maintain normal IOP engendered survival of retinal ganglion cells, whose loss is ultimately the cause for reduced vision in glaucoma. In vivo and in vitro analyses demonstrated higher TM cellularity in treated mice compared with littermate controls and indicated that this increase is primarily because of a proliferative response of endogenous TM cells. Thus, our study provides in vivo demonstration that regeneration of the glaucomatous TM is possible and points toward novel approaches in the treatment of this disease.

trabecular meshwork | glaucoma | iPSC | myocilin

Glaucoma is one of the most common causes of irreversible vision loss and blindness worldwide; ~60 million suffer from this disease, and of these, 7 million are blind (1). By definition all glaucoma involves some degree of vision loss, which is because of the death of retinal ganglion cells (RGC), as well as degeneration of the optic nerve head, the optic nerve, and the lateral geniculate nucleus (2, 3). Advanced age and elevated intraocular pressure (IOP) are the two most significant risk factors for the development of glaucoma. Elevated IOP is typically a result of disturbances in the balance of aqueous humor production and drainage. Aqueous humor is continuously synthesized within the eye and drained primarily through the trabecular meshwork (TM), a specialized structure located anterior to the root of the iris. Although occlusion of the aqueous humor outflow pathways can occur through several mechanisms, in the United States and other Western populations the most common form of glaucoma is primary open angle glaucoma (POAG), which manifests no gross abnormalities to the anterior portion of the eye.

Randomized clinical trials have shown that reduction of IOP slows the onset and progression of glaucoma, even in patients without suspicious elevation of IOP (4, 5). Although there has been increasing awareness that factors other than elevated IOP contribute to glaucomatous damage, to date all treatments for glaucoma remain aimed at reducing IOP either through surgical or medical means, which has resulted in significant preservation of vision and increased quality of life for millions of glaucoma patients (6, 7).

Although the TM in eyes with POAG appears relatively normal at a gross morphological level, a number of more subtle changes influencing the mechanical properties of the TM collagen beams and the accumulation of macromolecules have been observed that might increase outflow resistance (8, 9). The stiffness of the TM in eyes with glaucoma is significantly increased compared with that of normal TM and it is likely that reduced elasticity has significant ramifications on IOP maintenance (10, 11). Contraction and relaxation of the ciliary muscle and the resulting compaction and opening of the TM significantly affect aqueous humor outflow. Data have additionally demonstrated that contractile filaments in the TM cell cytoplasm exist, indicating that TM cells themselves may contract (12). Histologically, thickening of the trabecular beams and fusing of trabecular lamellae because of adhesions of the denuded portions of the trabeculae and accumulation of fibrillar plaque material in the juxtacanalicular tissue have been associated with POAG (13, 14).

The TM is populated by specialized postmitotic cells of mesenchymal origin. TM cells are gradually lost throughout life in all individuals and, under normal circumstances, they are not replaced (15). A number of studies have demonstrated that loss of TM cells is higher in POAG patients than in age-matched controls (16–18). The effects of lower TM cellularity are currently unclear, but it has been proposed that reduced TM cellularity, or the functional decline of surviving TM cells, engenders a reduced ability to maintain TM homeostasis and causes structural aberrations within the TM.

The notion that TM function can be restored in eyes with POAG is supported through studies of eyes having received laser trabeculoplasty, a technique that is frequently used for the management of elevated IOP in POAG. In this procedure, a laser is used to focally coagulate the uveal TM, resulting in diffuse stimulation of

Significance

The regulation of intraocular pressure (IOP) is vital for the health of the eye. Failure to maintain IOP frequently leads to vision loss in glaucoma. The IOP is maintained by the trabecular meshwork (TM), which exhibits decreased cellular density with age and disease. Here we demonstrate that induced pluripotent stem cells differentiated into TM cells (designated iPSC-TM) restore TM function for over 9 wk, regulate IOP, and prevent neuronal loss in a glaucoma mouse model. Transplanted iPSC-TM survive in the TM, but the most pronounced effect of transplantation is a robust proliferative response of endogenous TM cells. These findings suggest that lasting restoration of IOP control through iPSC-TM transplantation is possible and may represent a novel treatment approach for glaucoma.

Author contributions: W.Z., B.A.T., and M.H.K. designed research; W.Z., O.W.G., L.L., A.J., and J.M.T. performed research; L.L., A.J., V.C.S., J.M.T., B.A.T., and M.H.K. contributed new reagents/analytic tools; W.Z., O.W.G., L.L., A.J., V.C.S., J.M.T., B.A.T., and M.H.K. analyzed data; and W.Z., O.W.G., V.C.S., and M.H.K. wrote the paper.

The authors declare no conflict of interest.

This article is a PNAS Direct Submission. D.J.C. is a guest editor invited by the Editorial Board.

[1]To whom correspondence should be addressed. Email: markus-kuehn@uiowa.edu.

This article contains supporting information online at www.pnas.org/lookup/suppl/doi:10.1073/pnas.1604153113/-/DCSupplemental.

www.pnas.org/cgi/doi/10.1073/pnas.1604153113

TM cells (19, 20). One well-documented effect of laser trabeculoplasty is that it causes an increase in TM cell division, leading to the conclusion that the laser burn induces a repair process by repopulating a cell deficient TM (21, 22).

We previously demonstrated that induced pluripotent stem cells (iPSC) can be differentiated into a cell type, designated iPSC-TM, which resembles primary TM cells (pTM) (23). iPSC-TM are morphologically very similar to pTM, express a large number of proteins characteristic of TM, and functionally respond to various stimuli in a manner typical of TM cells. Herein we provide functional data to demonstrate that transplantation of iPSC-TM into a mouse model of glaucoma can restore IOP control and prevent RGC degeneration. These studies were aided by the development of a transgenic mouse model of glaucoma because of expression of human myocilin with the disease causing mutation Y437H (Tg-*MYOC*^{Y437H}) (24, 25). The eyes of these mice develop normally, and structural damage to the TM is modest, but significant loss of TM cells, elevated IOP, and subsequent RGC loss is observed as animals age (24). Thus, this mouse model provides an unparalleled opportunity to examine TM function following iPSC-TM transplantation. However, because loss and dysfunction of TM cells is observed in all forms of open angle glaucoma, it is possible that transplantation of iPSC-TM will be of benefit to a much larger group of individuals than those with mutations in *MYOC*.

Results

Preparation and Characterization of iPSC-TM. As we have shown previously, iPSC can be induced to differentiate into a cell type (iPSC-TM) that strongly resembles pTM morphologically, functionally, and compositionally (23). Here, mouse iPSC-TM were induced from iPSC derived from fibroblasts isolated from transgenic animals constitutively expressing the cellular marker dsRed. iPSC were seeded and, when confluency reached 5%, induced to differentiate by maintaining them in biopsy media previously conditioned by primary human TM cells. This approach induces distinct morphological changes in the cultured cells (Fig. 1*A*). iPSC grow in colonies of high cellular density and the ratio of nuclei to cytoplasm is much higher than that of other cells types. However, after 7-d differentiation, developing iPSC-TM have separated from the colonies, begin to exhibit spindle-like morphology, and resemble primary cultured TM cells although they are smaller at this stage. iPSC-TM continue to grow and after 14 d of differentiation are of similar size and exhibit the typical morphology of pTM.

The transition to an iPSC-TM phenotype is accompanied by profound changes in gene expression. After 14 d of differentiation, increasing numbers of iPSC-TM are immunopositive for laminin A4 (Lama4) and tissue inhibitor of matrix proteases 3 (Timp3), molecules that are prominently expressed in native TM cells, but not iPSC (Fig. 1*B*). These findings are supported by gene-expression analysis, demonstrating that expression of *Lama4* and *Timp3* increases during the transition from iPSC to iPSC-TM (Fig. 1*C*). Conversely, the iPSC biomarkers Nanog homeobox (*Nanog*) and SRY box 2 (*Sox2*) exhibit a progressive decrease in expression levels during this process.

We've also previously demonstrated that iPSC-TM respond to exposure to glucocorticoids with enhanced synthesis and secretion

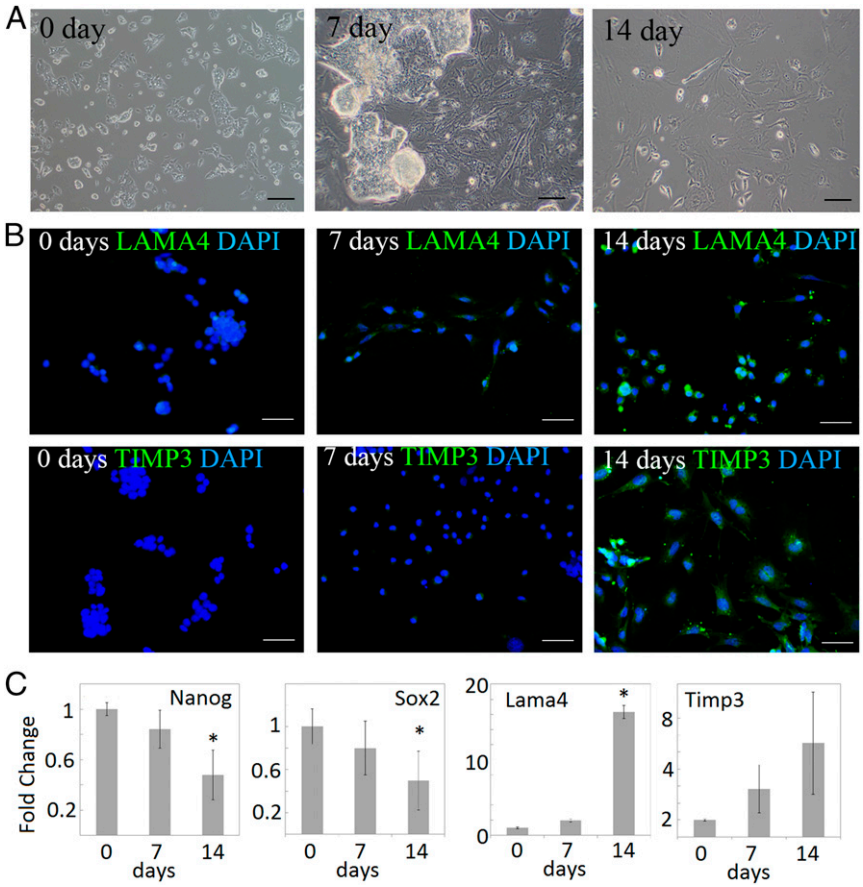

Fig. 1. Characterization of iPSC-TM. (*A*) Morphology of undifferentiated iPSCs (0 d) and iPSC-TM after 7- and 14-d differentiation. (*B*) Immunohistochemical detection of TM biomarkers LAMA4 and TIMP3 (green) in iPSC (0 d) and iPSCs-TM after 7- or 14-d differentiation. Nuclei were stained with DAPI (blue). (*C*) Fold-change of iPSCs biomarkers (Nanog and Sox2) and (LAMA4 and TIMP3) in iPSCs and iPSC-TM after 7- and 14-d differentiation. *$P < 0.05$. (Scale bars, 100 μm.)

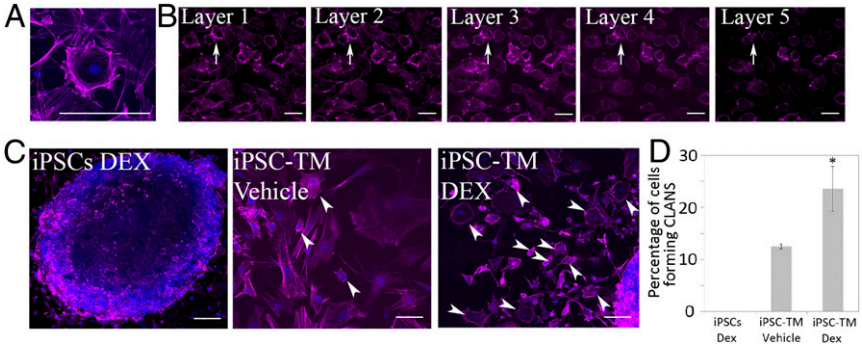

Fig. 2. Formation of CLANs in iPSC-TM. (*A*) High-magnification example of CLANs in iPSC-TM following 14-d differentiation and Dex treatment. Cells were stained with phalloidin and DAPI (blue). (*B*) Optical sections demonstrating the dome-shaped organization of iPSC-TM forming CLANs. The distance between each scan is 0.5 μm. An arrow has been inserted highlighting one cell to facilitate orientation. (*C*) Formation of CLANs in iPSC (*Left*) and 14 d differentiated iPSC-TM in the vehicle control (*Center*), and Dex treatment (*Right*) groups. Arrowheads highlight several, but not all, cells forming CLANs. (Scale bars, 100 μm.) (*D*) Quantitation of iPSC-TM forming CLANs in undifferentiated iPSC vehicle controls ($n = 3$) and Dex-treated cells ($n = 3$). *$P < 0.05$ vs. vehicle control.

of myocilin (23). Another well-characterized response of TM cells to glucocorticoid exposure is the formation of cross-linked actin networks (CLANs) (26). These cytoskeletal structures form geodesic dome-like polygonal lattices and can be discriminated from temporary arrangements of polygonal actin structures based on the cell's size and the height (Fig. 2 *A* and *B*). Previously published studies indicate that ~14% of human pTM and 30% of mouse pTM cells form CLANs (26, 27). Here, iPSC-TM were differentiated for 14 d and subsequently exposed to 100 nM dexamethasone (Dex) for 3 additional days. Controls included uninduced iPSC and iPSC-TM treated with vehicle only. Our findings demonstrate that CLANs are not observed in undifferentiated iPSC (Fig. 2*C*). However, Dex treatment of iPSC-TM resulted in CLAN formation in 23.62% ± 2.28 of all cells, whereas only 12.5% ± 0.48 of vehicle-treated iPSC-TM responded in this fashion ($P = 0.041$). These data provide additional support to our previous findings that our differentiation approach yields iPSC-TM that resemble pTM in many important aspects.

Purification of iPSC-TM. The formation of tumors as a result of the presence of remaining pluripotent cells is a significant safety concern for in vivo studies using iPSC. To produce iPSC-TM cells appropriate for transplantation, we used a negative-selection approach by removing cells still expressing markers of pluripotency from the iPSC-TM population. After differentiation for 14 d, stage-specific mouse embryonic antigen 1 positive (SSEA-1$^+$) cells were depleted using SSEA-1–conjugated magnetic beads. In our hands four successive rounds of purification are required to remove all SSEA-1$^+$ cells (Table 1). Elimination of these cells is a crucial aspect of this experimental approach. Transplantation of 50,000 iPSC-TM to the anterior chamber of normal recipient mice resulted in tumor formation in over 7% of all eyes using the twice-purified cell population containing 3% SSEA-1$^+$ cells. However, four rounds of purification effectively removed all SSEA-1$^+$ cells and transplantation of this fraction did not result in tumor formation in any of the treated mice.

iPSC-TM purified in this manner can be further maintained in vitro. iPSC-TM continue to express the dsRed transgene and retain a morphological appearance similar to pTM cells (Fig. S1). These data demonstrate that meticulous removal of iPSC with remaining pluripotency is essential for use in vivo but also that multiple rounds of magnetic separation are effective in creating a stable and safe population of cells for transplantation.

Time Course of Damage in Tg-*MYOC*^{Y437H} Mice. These studies relied on the use of a transgenic mouse model of glaucoma. These animals constitutively express human myocilin harboring a pathogenic mutation (Tg-*MYOC*^{Y437H}) and display multiple glaucomatous phenotypes, including TM cell loss, elevated IOP, and progressive RGC loss (24). To further define the pathological stages of this mouse model and to identify a suitable age for transplantation, we improved upon our previously published data (24) by obtaining detailed data for IOP, aqueous humor outflow facility, and TM cellularity in 2-, 4-, and 6-mo-old Tg-*MYOC*^{Y437H} mice, as well as in age-matched WT littermate controls (Fig. 3*A*). Congruent with our previous findings, IOP in 2-mo-old Tg-*MYOC*^{Y437H} mice does not differ from that observed in control animals. However, IOP does increase with age in transgenic mice and, although IOP is slightly elevated at age 4 mo (15.1 mmHg vs. 13.9 mmHg, $P = 0.037$), the difference becomes readily apparent by age 6 mo (15.8 mmHg vs. 13.9 mmHg, $P = 0.0019$).

Measurements of aqueous humor outflow facility are more sensitive in unmasking subtle disturbances in aqueous humor drainage. We used this approach in the same groups of control and Tg-*MYOC*^{Y437H} mice (Fig. 3*B*). As reported elsewhere (28), we observed comparatively low outflow facility in young animals. In WT mice aqueous humor outflow facility increases between 2 and 4 mo of age (0.016 ± 0.008 and 0.029 ± 0.006 μL·min·mmHg, respectively) but remains stable thereafter (0.030 ± 0.013 μL·min·mmHg in 6-mo-old WT mice). In Tg-*MYOC*^{Y437H} mice outflow facility resembles that of young normal mice at a young age (0.017 ± 0.009 μL·min·mmHg) but, analogous to our observations for IOP, deficiencies become apparent in 4-mo-old animals (0.024 ± 0.011 μL·min·mmHg) and are statistically significant by age 6 mo (0.014 ± 0.0007 μL·min·mmHg, $P = 0.0124$).

The development of aqueous humor outflow deficiencies is accompanied by a progressive decrease in the cellular density of the TM. Although the anterior segment, including the TM, develops normally in transgenic animals, expression of *MYOC*^{Y437H} leads to endoplasmic reticulum stress and TM cell loss (24). To further define this process, we determined TM density, defined as nuclei contained within the collagen IV immunoreactive tissue overlying the Schlemm's canal in 4- and 6-mo-old Tg-*MYOC*^{Y437H} and control mice (Fig. 3*C*). Data obtained demonstrate that at the

Table 1. Purification of SSEA-1$^+$ cells

Rounds of purification	SSEA-1$^+$ cell ratio (%)	Teratoma formation
1	39.2	66.6% (8/12)
2	3.0	7.14% (1/14)
3	0.0	0.0% (0/14)

Quantitation of SSEA-1$^+$ cells after one, two, and four rounds of purification and corresponding tumor formation ratios following anterior chamber injection in Tg-*MYOC*^{Y437H} mice ($n = 12$, 14, and 14, respectively).

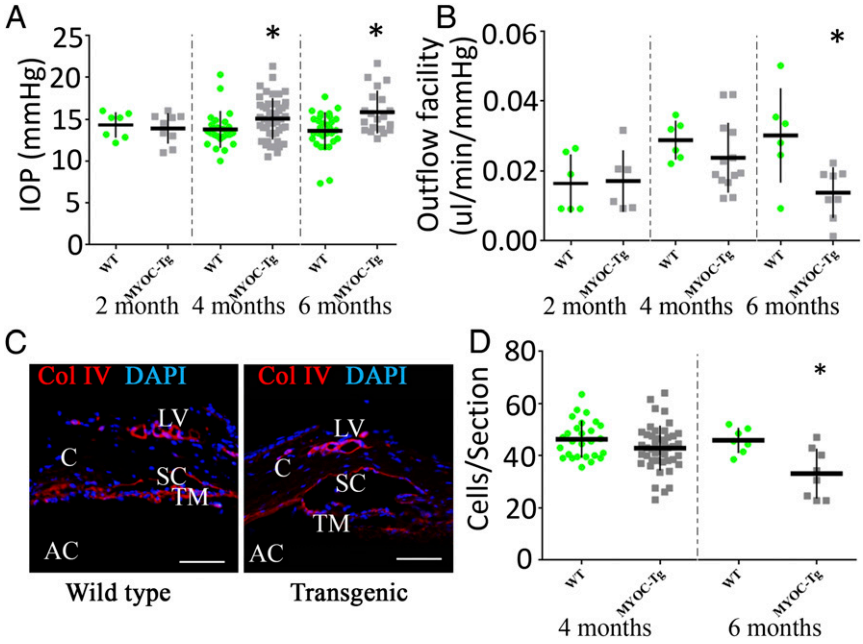

Fig. 3. Development of pathology in Tg-*MYOC*^{Y437H} mice. (*A*) IOP in 2-, 4-, and 6-mo-old Tg-*MYOC*^{Y437H} mice (n = 9, 47, and 20, respectively) and age-matched WT littermates (n = 7, 24, 31, respectively). (*B*) Outflow facility in 2-, 4-, and 6-mo-old Tg-*MYOC*^{Y437H} mice (n = 6, 13, and 8, respectively) and age-matched controls (n = 6, 6, and 6, respectively). (*C*) Immunohistochemical detection of collagen IV (Col, red) and DAPI (blue) in the anterior segment of 6-mo-old WT and *MYOC* transgenic (Tg) mice. For the purpose of this study, the TM is defined as the Col IV^{+} region overlying the Schlemm's canal. (*D*) Quantitation of TM cells number in 4- and 6-mo-old Tg-*MYOC*^{Y437H} mice (n = 26 and 8, respectively) and age-matched controls (n = 14 and 6, respectively). *P < 0.05. (Scale bars, 100 μm.)

age of 4 mo very few TM cells have been lost in transgenic animals (42.8 ± 8.6 cells vs. 46.3 ± 7.1 cells, P = 0.09), but a marked loss is readily apparent at 6 mo (33.1 ± 9.5 cells vs. 45.8 ± 4.8 cells, P = 0.007) (Fig. 3*D*). The age of pronounced TM cell loss is consistent with that at which functional deficits become apparent and further demonstrates that the disruption of outflow facility in Tg-*MYOC*^{Y437H} mice is a degenerative process, as opposed to a developmental deficit. Minor effects of the mutation are apparent at 4 mo of age, suggesting the onset of the degenerative process, but disruption of aqueous humor dynamics accelerates thereafter and becomes statistically significant in all parameters evaluated here.

iPSC-TM Transplantation in Vivo. Based upon our observation that 4-mo-old Tg-*MYOC*^{Y437H} mice exhibit the first signs of TM cell loss, we sought to determine whether aqueous humor dynamics can be preserved through the transplantation of iPSC-TM derived from healthy mice. Therefore, 50,000 purified iPSC-TM were injected into the anterior chamber of 4-mo-old Tg-*MYOC*^{Y437H} mice in a volume of 3 μL PBS (n = 22). Additionally, we injected an equal number of fibroblasts, a cell type known to secrete growth factors that can support TM cell survival, in a second group of transgenic mice (n = 8). Transgenic animals receiving an injection of an equal volume of PBS served as controls (vehicle control, n = 16). In addition, age-matched WT mice (n = 20) were used. IOP and outflow facility were determined before transplantation, as well as 6 and 9 wk after injection (5.5 and 6.25 mo of age).

Consistent with the data shown above, the group of transgenic animals used for these transplantation studies displayed minor differences in IOP at the age of 4 mo compared with the WT controls (14.4 ± 1.8 mmHg vs. 13.6 ± 1.6 mmHg) (Fig. 4*A*). Similarly, whereas minor differences in the aqueous humor outflow facility were apparent, statistical significance was not yet reached (0.024 ± 0.01 vs. 0.029 ± 0.006 μL·min·mmHg, P = 0.2) (Fig. 4*B*). As expected, 6-wk later the IOP had risen and the aqueous humor outflow facility had markedly decreased in vehicle control-injected transgenic animals (16.4 ± 3.1 mmHg and 0.014 ± 0.005 μL·min·mmHg). In contrast, IOP and outflow facility in iPSC-TM recipient eyes resembled that of WT mice (12.6 ± 3.7 mmHg and 0.025 ± 0.01 μL·min·mmHg) and were significantly better that those determined in the vehicle control group (P = 0.001 and 0.02, respectively). IOP remained significantly lower in iPSC-TM–treated animals than in vehicle control mice until the last measurement was taken 9 wk after transplantation (12.2 ± 2.8 mmHg, P = 0.0006). At this point, aqueous humor outflow facility also continued to be significantly higher in iPSC-TM recipient animals compared with PBS control mice (0.027 ± 0.01 vs. 0.011 ± 0.005 μL·min·mmHg, P = 0.017).

Transplantation of fibroblasts provided a minor improvement of IOP and outflow facility, although a statistically significant rescue effect compared with the vehicle control group could not be demonstrated for either measure. IOP and outflow facility in these mice were at 14.5 ± 3.5 mmHg (P = 0.15) and 0.022 ± 0.01 μL·min·mmHg (P = 0.09) 6 wk after transplantation. After 9 wk, IOP had slightly increased (14.6 ± 3.0 mmHg, P = 0.17) and outflow facility declined to 0.016 ± 0.013 μL·min·mmHg (P = 0.45). However, because of the slightly improved outflow dynamics, values obtained in fibroblast-injected mice are also not statistically different from those of WT mice (P = 0.27 and 0.22 for outflow facility and 0.7 and 0.6 for IOP at 6 and 9 wk, respectively).

Reduction of IOP to achieve RGC survival is a mainstay of clinical glaucoma therapy. Importantly, in iPSC-TM recipient eyes the reduction of IOP also resulted in RGC rescue. Mice were killed 12 wk after transplantation and surviving RGC were identified through γ-synuclein immunoreactivity (Fig. 4*C*). Although this approach relies on continuous expression of this RGC marker, we and others have found a high correlation between RGC numbers and optic nerve damage (24, 29–34). Data obtained here demonstrate that eyes of vehicle control Tg-*MYOC*^{Y437H} animals display a significantly lower RGC density than those of WT controls (1706.9 ± 491.3 RGC/mm^2 vs. 2171.9 ± 186.3 RGC/mm^2, P = 0.027). In contrast, iPSC-TM recipient eyes of transgenic mice display a RGC density similar to WT mice and significantly higher density then the vehicle control group (2222.1 ± 250.4 RGC/mm^2, P = 0.041). A protective effect was not apparent in the fibroblast group (1675.6 ±

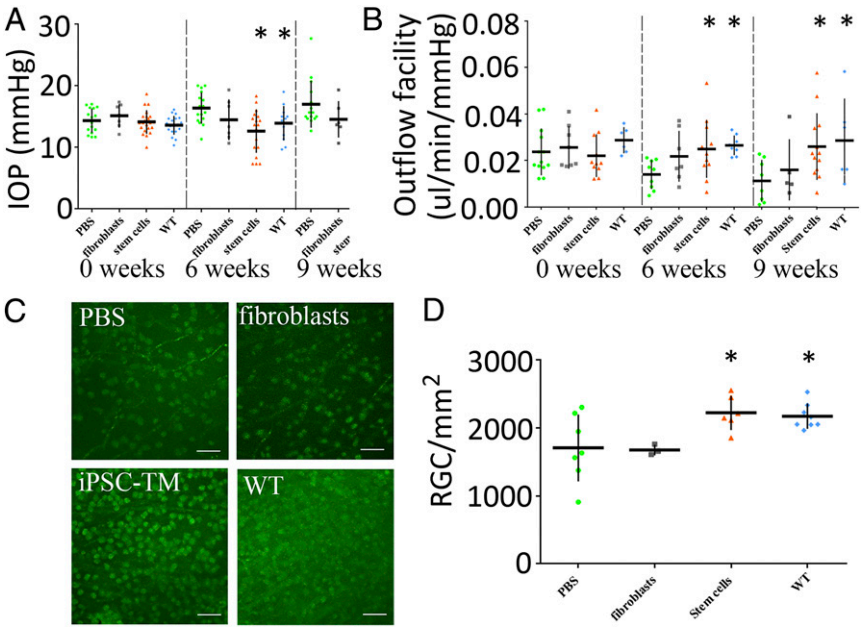

Fig. 4. Functional rescue of glaucoma phenotypes through iPSC-TM transplantation. IOP (*A*) was determined in Tg-*MYOC*^{Y437H} mice having received either PBS (n = 15–16), fibroblasts (n = 6–7), or iPSC-TM (n = 18–22), as well as in WT mice (n = 12–18). Measurements were taken before transplantation (0 wk), and 6- and 9-wk posttransplantation. (*B*) Determination of aqueous humor outflow facility in transgenic mice receiving either PBS (n = 8–13), fibroblasts (n = 6–8), or iPSC-TM (n = 12–13), or WT mice (n = 7–8). (*C*) Examples of immunohistochemical detection of γ-synuclein^{+} RGC in whole-mounted retinas 12 wk after transplantation. (*D*) Quantitation of RGC in mice having received transplantation of PBS (n = 7), fibroblasts (n = 4), or iPSC-TM (n = 6), as well as WT mice (n = 8). *P < 0.05. (Scale bars, 100 μm.)

77.6 RGC/mm^2, P = 0.92) (Fig. 4*D*). Taken together, these data demonstrate that intraocular injection of iPSC-TM prevents IOP elevation and aqueous humor outflow reduction and results in preservation of RGC density in Tg-*MYOC*^{Y437H} mice.

Cellular Effects of iPSC-TM in Vivo. To estimate iPSC-TM survival in vivo and to gain insight into the consequences of transplantation, we determined both native TM cell and iPSC-TM density in study animals. The immunohistochemical analysis of sagittal sections of the anterior segment of iPSC-TM recipient eyes demonstrate that iPSC-TM integrate into the TM and survive for at least 12 wk until the end of the study period (Fig. 5*A*). Off-target integration was also detected in other tissues of the anterior chamber, such as the endothelial cell layer of the Schlemm's canal, and the corneal epithelium and stroma, particularly in the area surrounding the injection site. However, there are no indications that these cells compromise the function of the recipient eyes.

Histochemical evaluation of recipient eyes suggested that iPSC-TM treatment results in slight hypertrophy of the TM (Fig. S2). To quantify the number of implanted iPSC-TM and endogenous TM cells in vivo we determined both the number of total nuclei in the TM as well as the number of nuclei of dsRed immunopositive cells in all experimental groups. Here, the TM was defined as the collagen IV immunoreactive tissue overlying the Schlemm's canal. As expected, vehicle control animals exhibited a marked loss of TM cell density compared with WT animals (25.7 ± 7.3 TM per section vs. 57.1 ± 12.1 TM per section, P = 0.00014) (Fig. 5*B*). Injection of fibroblasts again resulted in a slight improvement, but did not result in a significant increase (38.7 ± 1.5 TM per section, P = 0.09). In contrast, the cellular density of the TM in transgenic iPSC-TM recipient mice was significantly higher than that of vehicle controls (54.9 ± 7.2 TM per section, P = 6.83E-06) and similar to that of WT animals. Interestingly, although sections of iPSC-TM recipient mice contained on average 29.3 more cells per

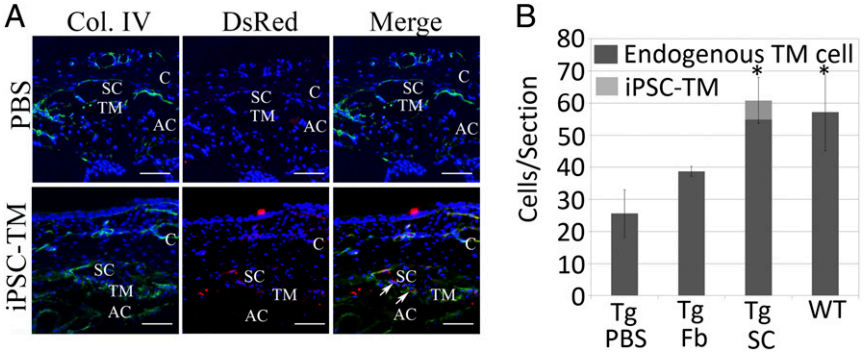

Fig. 5. Quantification of iPSC-TM and primary TM cell survival. (*A*) Immunohistochemical detection of Col IV (green, left column), dsRed (red, center column) and DAPI (blue) in anterior segment of PBS (*Upper*) or iPSC-TM (*Lower*) recipients at 12 wk after injections. (*B*) Quantitation of implanted iPSC-TM and endogenous TM cells in PBS recipients (Tg PBS, n = 5), fibroblasts recipients (tg-Fb, n = 3), iPSC-TM recipients (SC, n = 7), and WT mice (n = 10) at 12-wk posttransplantation. Implanted iPSC-TM were stained with ds Red antibody (red) and are represented by the lightly shaded portion in the bar graph. Nuclei were labeled with DAPI (Blue). *P < 0.05. (Scale bars, 100 μm.)

section than those of animals having received PBS injection, we observed on average only 5.9 dsRed$^+$ cells in each of the sections. This finding suggests that the majority of the additional cells observed in iPSC-TM recipients are not transplanted; rather, they are endogenous cells that have either survived or were replaced through division of the remaining cells.

Proproliferative Effect of iPSC-TM in Vitro. To determine if iPSC-TM exert a proproliferative effect on normal mouse pTM cells, we conducted a series of in vitro experiments. Cultures of pTM (27) were infected with adenoviral vectors expressing the same myocilin construct as in the transgenic mice (Ad5RSV-myocilin^{Y437H}). Expression of this mutated protein has been reported to result in cellular stress and reduced cell survival (35–37).

Congruent with these findings, we observed slightly reduced growth rates in transfected pTM cells (Fig. 6*A*): 50,000 untreated pTM cultured in media alone proliferated to 81,558 ± 4,038 cells within 4 d. The growth rate of pTM infected with Ad5RSV-myocilin^{Y437H} is slightly reduced compared with the control (69,383 ± 3,017 or 85.1%, $P = 0.032$). However, when Ad5RSV-myocilin^{Y437H}–infected pTM were cultured in direct contact with iPSC-TM, they exhibited distinctly higher growth rates than the control cells. Cultures seeded with 50,000 Ad5RSV-myocilin^{Y437H}–infected pTM and 50,000 dsRed$^+$ iPSC-TM contained 212,264 ± 3,147 cells after the 4-d growth period. Of these, only 22,522 ± 6,122 (10.6%) cells are dsRed$^+$ iPSC-TM cells, whereas 189,742 ± 34,600 (89.4%) are pTM. This finding represents a substantially elevated growth rate (232% of control), even compared with nonvector-treated control cells maintained without iPSC-TM ($P = 0.004$).

A similar proproliferative effect was not observed when iPSC-TM are physically separated from the pTM through the use of cell culture inserts, allowing only the conditioned media to interact with the pTM (Fig. 6*B*). Ad5RSV-myocilin^{Y437H}–infected pTM maintained either in unconditioned media or media conditioned through coculture with iPSC-TM exhibit replication rates similar to control cells (83.4% and 99.8% of control, respectively).

The notion that direct contact with iPSC-TM leads to enhanced proliferation of pTM was further supported by analysis of incorporation rates of the thymidine analog BrdU (Fig. 6*C*). In the absence of iPSC-TM 21.3% ± 8.2 of pTM are BrdU$^+$ after 2 h, whereas coculture increases this fraction to 32.8% ± 12.4 of all (dsRed$^-$) pTM ($P = 0.032$). These data indicate that direct contact between iPSC-TM and the target cell is required to initiate enhanced proliferation rates in pTM.

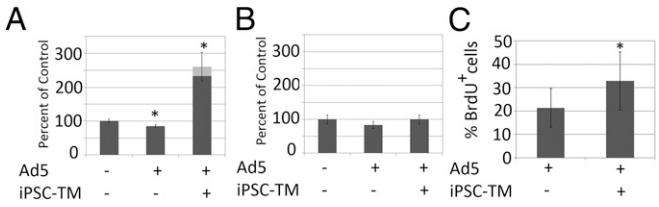

Fig. 6. Proproliferative effect of iPSC-TM in vitro. (*A*) Growth rates of pTM cells after 4 d in culture. pTM infected with Ad5RSV-myocilin^{Y437H} exhibit slightly reduced growth compared with untreated controls whereas vector treated cells in the presence of iPSC-TM grow much more quickly than controls ($n = 3$). Dark shaded segments indicate the percentage of pTM (unlabeled); lightly shaded segments indicate percentage of iPSC-TM (dsRed$^+$). (*B*) Growth of pTM physically separated from iPSC-TM. After 4 d in culture, pTM treated with Ad5RSV-myocilin^{Y437H}, grown in the presence or absence of iPSC-TM exhibit growth rates similar to untreated control cells ($n = 3$). (*C*) Percentage of actively dividing Ad5RSV-myocilin^{Y437H} treated pTM as indicated by incorporation of BrdU. Direct contact with iPSC-TM significantly enhances the fraction of BrdU positive pTM ($n = 3$/group). *$P < 0.05$.

In Vivo Transcriptional Analysis. The above findings suggest that the observed functional rescue in Tg-myocilin^{Y437H} mice is a result of the re-entry of normally nonmitotic endogenous TM into cell division following stimulation by iPSC-TM. To further support this hypothesis and to gather evidence for proliferation in our in vivo model, we carried out global gene-expression analysis of the TM of Tg-myocilin^{Y437H} mice harvested 12 wk after receiving iPSC-TM, fibroblasts, or vehicle control injections. A total of 879 genes exceeded the cut-off criteria (expression fold-change > 1.5 and $P < 0.01$) and grouped into 83 clusters based upon their expression profile (Fig. 7*A*). For subsequent Gene Ontology analysis, only genes assigned to clusters containing at least three genes and with a confidence value above 28 were selected (Fig. 7*B*). Analysis of these 792 genes by the Panther Classification System (38) identified 265 genes whose functions are related to cellular processes, including cell communication (129 genes) and cell cycle (56 genes) (Dataset S1). These data add further support to the notion that the presence of iPSC-TM induces proliferation and that this effect can be maintained for an extended period.

Discussion

The IOP depends on the balance between aqueous humor production by the ciliary body and drainage through the TM. In the normal eye, resident endothelial cells of the TM maintain its structure by continuously remodeling the TM beams and by degrading debris that might otherwise accumulate and occlude the outflow pathways. Loss of TM cells has been suspected to contribute to aqueous humor outflow deficiencies and, conversely, it has been hypothesized that replacing lost cells can restore function to the eye (39). Previous studies by this and other laboratories have indicated that either multipotent cells isolated from the TM (40, 41) or iPSC may be useful for this purpose (23, 42). Indeed, recently published data have indicated that iPSC can restore some functional aspects in an organ culture system. Our study demonstrates that TM-like cells, derived from iPSC, can functionally rescue a glaucoma phenotype in mice. These studies were aided to a large degree by the availability of the myocilin mouse model of glaucoma. As previously described, these transgenic animals express a pathogenic form of human myocilin, which causes endoplasmic reticulum stress, TM cellular dysfunction, and cell loss (24). However, the anterior segment, including the TM, develops normally in these mice and disturbances in aqueous humor outflow dynamics only become apparent as the animals age. Importantly, similar to human POAG, the pathophysiological events leading to reduced aqueous humor outflow are not associated with gross morphological disruption of the aqueous humor drainage structures, as is the case in many surgically induced models or those resulting from congenital anterior segment malformation (33, 43). Thus, we reasoned that the TM in these mice will be amenable to restoration. For the reported studies 4-mo-old recipient animals were chosen. At this age, the first signs of a disturbance in the aqueous humor dynamics become apparent in some individuals, including modest elevation of IOP and decreased outflow facility. In untreated mice, the symptoms worsen over the next few weeks and, at the age of 6 mo, the vast majority of transgenic mice develop mildly elevated IOP, significantly reduced aqueous humor outflow facility, and a clear reduction in TM cellularity.

Our data demonstrate that transplantation of iPSC-TM into the eyes of 4-mo-old Tg-*MYOC*^{Y437H} mice prevents the development of elevated IOP and preserves normal aqueous humor normal outflow facility for at least 9 wk. This effect cannot be achieved through transplantation of fibroblasts. These cells would represent a convenient source of patient-derived material and secrete growth factors, such as EGF and PDGF, that stimulate TM cell proliferation (44, 45). Furthermore, fibroblasts closely resemble mesenchymal stromal cells that have shown promise in laser-induced models of glaucoma (46, 47). Our findings indicate that these cells are not inert and improve TM function to some degree. However, a statistically

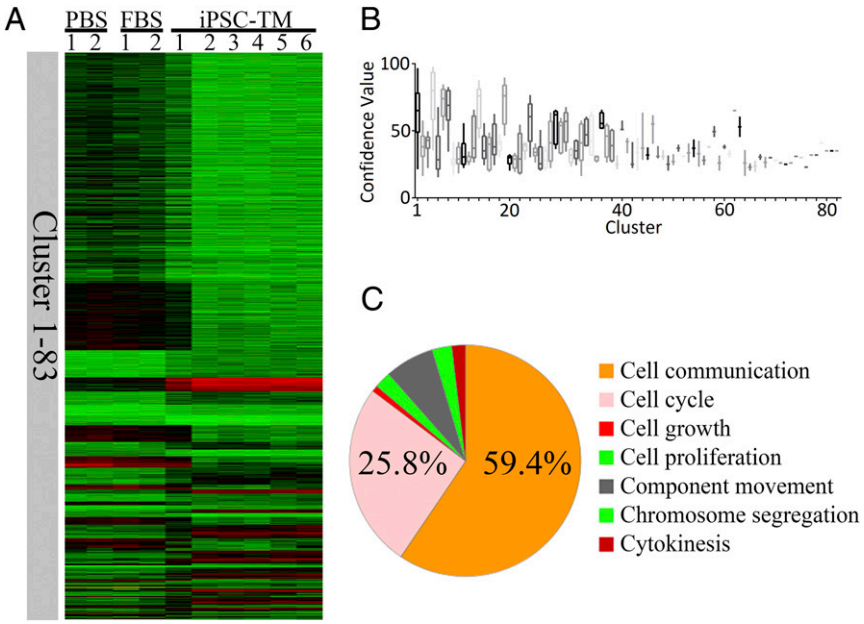

Fig. 7. Transcriptional analysis of mouse TM after transplantation. (*A*) Heatmap of clusters generated by AutoSOME, demonstrating the distinct expression profile in eyes having received iPSC-TM (SC) compared with those having received injections containing either vehicle only (PBS) or fibroblasts (FBS). Here, green color designates high values, red low values. (*B*) Distribution of confidence values for the genes in each AutoSOME cluster. Confidence values designate the gene's likelihood to be grouped within this cluster during ensemble runs. (*C*) Distribution of gene ontology associations by the Panther Classification System.

significant rescue effect cannot be demonstrated. Importantly the prevention of RGC loss, which is the ultimate cause of vision loss in glaucoma, can only be demonstrated in iPSC-TM treated eyes.

Immunohistochemical evaluation of the anterior segment of treated and control eyes revealed that transplanted iPSC-TM frequently become established in the TM of recipient eyes and survive for at least 12 wk. Transplanted cells were also observed in other tissues of the anterior segment, in particular the iris and corneal endothelium, but this did not noticeably impair these tissues. Furthermore, whereas early transplantation attempts using iPSC-TM populations containing small amounts of cells retaining expression of SSEA-1 frequently led to the formation of ocular tumors, the scrupulous removal of any such cells prove to be a viable and safe approach.

In the adult eye, TM cells do not proliferate under normal circumstances. One possible scenario how iPSC-TM might achieve functional restoration of the TM may be that the transplanted cells establish themselves within the tissue and carry out functions typically carried out by the endogenous cells. It is conceivable that, at least in part, this is also the case here. However, although we observed a strikingly higher TM cell density in transplanted eyes compared with control eyes, the majority of these additional cells are not iPSC-TM, but are derived through division of the recipient eyes' endogenous TM cells. Thus, a significant benefit of iPSC-TM transplantation is that this process causes endogenous TM cells to re-enter the cell cycle and replace previously lost cells. Accordingly, we detect increased expression of a number of genes associated with cellular division in eyes having received iPSC-TM. This proliferation-enhancing effect of iPSC-TM can also be demonstrated in vitro. Coculture of pTM cells with iPSC-TM results in significantly higher proliferation rates than those observed in pTM alone. Although the mechanism remains currently unresolved, our data demonstrate that it requires cell–cell contact as coculture of physically separated iPSC-TM, and pTM does not replicate the effect.

It is interesting to note that earlier studies examining the physiological consequences of laser trabeculoplasty, a treatment approach using mild laser stimulation of the TM, had also noted an increase in the number of TM cells in the treated areas that the investigators had speculated might be the cause of improved aqueous humor outflow (21, 22). The newly derived TM cells are derived from a population of progenitor cells located directly beneath the Schwalbe's line that are suspected to resemble stem cells (48). It is intriguing to speculate whether the endogenous TM cells re-entering the cell cycle following iPSC-TM transplantation belong to this particular TM cell subtype. On the other hand, the normally postmitotic TM cells of the adult eye retain some proliferative properties and readily divide in vitro. Thus, it is conceivable that iPSC-TM–mediated signaling removes proliferative inhibition and causes cell division in vivo.

Although these studies are very encouraging, a number of questions remain. For example, because the functional restoration appears to depend upon proliferation of endogenous TM cells, which also express *MYOC*^{Y437H}, it is possible that these newly derived cells are themselves eventually lost resulting in a gradual return of outflow dysfunction. Although in theory eyes can be retreated with iPSC-TM, the influence of advanced age is currently unclear. It is conceivable that this approach is less successful in very old eyes. These considerations may be less of a concern in cases of open angle glaucoma that are not the result of this very aggressive mutation, because TM cell loss typically occurs over many decades and, assuming similar rates of cell loss, newly derived TM cells may survive for many years. However, additional studies will have to be carried out to determine whether this approach can be successfully used to reverse aqueous humor outflow deficiencies in other animal models or in other types of glaucoma. We are confident that the TM cell loss exhibited in our mouse model shares many important features with general POAG. Other types of glaucoma (e.g., that associated with pseudoexfoliation syndrome) result from dissimilar damage to the TM, and it will be interesting to determine if our approach will also be beneficial in these cases.

Materials and Methods

Additional experimental details are included in *SI Materials and Methods* and Tables S1–S3.

Mice. Tg-*MYOC*^{Y437H} breeder mice were maintained on a C57BL/6J background. Experimental animals were generated by crosses between these and SJL/J mice and only F1 animals were used.

Generation and Differentiation of iPSC. Mouse iPSC were generated by reprogramming fifth passage fibroblasts of 6-wk-old transgenic mice expressing the marker protein dsRed [B6.Cg-Tg(ACTB-DsRed*MST)1Nagy/J, Jackson Laboratory] using a set of ecotropic retrovirus (mouse OKSM), as described previously (49, 50). Mouse iPSC were cultured on 0.2% matrigel coated plates in mouse iPSC media [DEME/F12, 15% (vol/vol) heat-inactivated FBS, 1% NEAA, 1% L-glutamine, 1% Pen/Strep, 0.2% Fungizone, 0.0008% BME], which was exchanged daily.

Mouse iPSC were differentiated through culture in media preconditioned by human pTM. Briefly, human pTM were isolated from the TM of donor eyes, as described previously (51) and cultured in Biopsy media (MEM-α, 10% inactivated FBS, 0.2% primocin). The media conditioned by these pTM was collected daily, pooled, and sterilized by filtration through MCE membrane filters (0.2-μm pore size; Millipore). Sterilized conditioned media was used to induce iPSC to differentiate once the confluency of iPSC reached 5% and the media was exchanged daily.

Induction of CLANs. Mouse iPSC were differentiated for 14 d and then exposed with 100 nM Dex for 3 d. Control cells were treated with 1% ethanol (vehicle control). Cells were stained with Alexa Fluor 647 Phalloidin and 16 100× images were taken from each sample. Nuclei of all iPSC-TM forming CLANs, defined as cytoskeletal structures as geodesic dome-like polygonal lattices in dome-shaped cells, were counted and compared with the fraction of all iPSC-TM present.

Purification of iPSC-TM. Following 14 d of differentiation, 10^7 cells were trypsinized, resuspended and incubated with magnetic microbeads conjugated to SSEA-1 (CD15) antibodies (Miltenyi Biotec). Cells were washed and loaded into a MACS LD column placed in the magnetic separator (Miltenyi Biotec). See *SI Materials and Methods* for details.

iPSC Transplantation. Mice were deep anesthetized using a ketamine/xylazine mixture (87.5 mg/kg ketamine and 12.5 mg/kg xylazine). Next, 50,000 iPSC-TM in 3 μL PBS were injected into the anterior chamber through the cornea in the limbal region using 33-gauge half-inch stainless steel needles. Immediately before injection, a small amount of aqueous humor was allowed to escape to accommodate the injected volume. An equal volume of PBS was injected in the control group. GenTeal Severe Dry Eye Relief Lubricant was applied on the surface of the cornea after the injections to avoid excessive drying during the anesthesia.

IOP Measurements. IOP was measured between 9:00 AM to 12:00 PM using a rebound tonometer (TonoLab, Colonial Medical Supply). Mice were anesthetized by 2.5% (wt/vol) isoflurane plus 80% (vol/vol) oxygen for 5 min before IOP measurements, as described previously (52). IOP data were collected in a double-blind manner from all animals.

Aqueous Humor Outflow Facility Measurement. Measurements were carried out in live mice using approaches similar to those described previously (53–55). Mice were deep-anesthetized and the anterior chamber was cannulated with a 33-gauge stainless-steel needle connected to a flow-through pressure transducer (IcuMedical). A 100-μL Hamilton syringe containing 0.9% saline was loaded in a programmable pump. Data from the pressure transducer is transferred to a computer and analyzed by HemoLab software (Stauss Scientific). The software also controls the syringe pump and adjusts the pump rates to achieve the desired pressures. Rates were recorded at 15 mmHg, 25 mmHg, and 35 mmHg IOP for at least 7 min each (Fig. S3). Average flow rates for each pressure were determined and used to calculate the aqueous humor outflow facility, defined as microliter per minute per millimeter of mercury. Data were only considered acceptable if a stable measurement was attained at all pressure steps and a r^2 value > 0.95 was reached. To minimize the number of manipulations carried out on each eye, not all transplanted eyes were assessed at all time points.

Immunohistochemistry. Cells were grown on coverslips and fixed in 4% (wt/vol) paraformaldehyde for 20 min. Animal tissues were fixed in 4% paraformaldehyde for 4 h, embedded in OCT, frozen, and sectioned to 10-μm thickness on a cryostat. See *SI Materials and Methods* for additional details.

Morphometric Studies. To count dsRed iPSC-TM cells and endogenous TM cells in vivo, anterior chambers were sectioned to 10-μm thickness. TM tissues were identified by collagen IV immunoreactivity (Abcam) and iPSC-TM cells were labeled with dsRed antibody (Santa Cruz). Nuclei were stained using 0.1 μg/mL DAPI (Life Technologies). For each sample, nuclei of iPSC-TM cells and endogenous TM cells from nine sections were counted and the numbers were averaged.

To determine RGC density, eyes were enucleated and retinas were carefully dissected. Retinas were incubated overnight with antibodies directed against γ-synuclein (Abnova). After several rinses and the application of donkey anti-mouse secondary antibody (Life Technologies), retinas were whole-mounted. Eight 40× images each representing an area of 318 × 318 μm^2 were taken at predetermined locations representing the whole retina. RGC were counted in each image and data were averaged. One caveat of this approach is that only γ-synuclein RGC are identified.

In Vitro Studies. Mouse pTM were transfected with adenoviral vectors expressing either a pathogenic form of human myocilin (Ad5RSVmyocilin^{Y437H}HisFlag) or empty Ad5CMV (control). The effects of cell–cell contact with iPSC-TM and pTM was determined by seeding 50,000 purified iPSC-TM cells in transwell inserts above 50,000 mouse pTM. Alternatively, 50,000 mouse pTM were maintained in the presence of 50,000 iPSC-TM. The number of surviving cells was determined using flow cytometry analysis.

For proliferation studies, mouse pTM were infected with Ad5RSV-myocilin^{Y437H}HisFlag as above and grown in the presence of 10 μM BrdU for 2 h. BrdU incorporation was detected by immunohistochemistry. The experiment was carried out in triplicate. See *SI Materials and Methods* for additional details.

Global Gene Expression Analysis. For global transcriptional analysis of mouse anterior segments, tissue was harvested from treated and control eyes 12 wk after transplantation. Samples were hybridized to Affymetrix mouse 430 2.0 microarrays using standard Affymetrix protocols, as described previously (56). For subsequent analysis, data from mice having received either PBS or fibroblast injections were grouped and compared with those derived from iPSC-TM recipients. Cut-off values of 1.5 fold-change in expression levels and $P < 0.01$ were chosen. These data were grouped into clusters using AutoSOME and the biological function of clusters was determined by the Panther Classification System. See *SI Materials and Methods* for additional details.

Statistical Analysis. Student's *t* test was used for statistical evaluation between two groups. *P* values < 0.05 were considered to be significant throughout this investigation.

Study Approval. All animal experimentation was carried out in accordance with the NIH *Guide for the Care and Use of Laboratory Animals* (57) and all protocols were reviewed and approved by the University of Iowa committee on Animal Care and Use.

ACKNOWLEDGMENTS. The authors thank Dr. Qiong Ding, Ms. Amy Cook, Mr. Cole Starkey, and Mr. Cory Christensen for their help with these studies. This work was supported in part by Merit Review Award I01 RX001163 from the US Department of Veterans Affairs Rehabilitation R&D (Rehab RD) Service, and Research to Prevent Blindness (to M.H.K.).

1. Quigley HA, Broman AT (2006) The number of people with glaucoma worldwide in 2010 and 2020. *Br J Ophthalmol* 90(3):262–267.
2. Kuehn MH, Fingert JH, Kwon YH (2005) Retinal ganglion cell death in glaucoma: Mechanisms and neuroprotective strategies. *Ophthalmol Clin North Am* 18(3):383–395, vi.
3. Gupta N, Yücel YH (2007) Glaucoma as a neurodegenerative disease. *Curr Opin Ophthalmol* 18(2):110–114.
4. Heijl A, et al.; Early Manifest Glaucoma Trial Group (2002) Reduction of intraocular pressure and glaucoma progression: Results from the Early Manifest Glaucoma Trial. *Arch Ophthalmol* 120(10):1268–1279.
5. Kass MA, et al. (2002) The Ocular Hypertension Treatment Study: A randomized trial determines that topical ocular hypotensive medication delays or prevents the onset of primary open-angle glaucoma. *Arch Ophthalmol* 120(6):701–713; discussion 829–730.
6. Alward WL (1998) Medical management of glaucoma. *N Engl J Med* 339(18):1298–1307.
7. Weinreb RN, Khaw PT (2004) Primary open-angle glaucoma. *Lancet* 363(9422):1711–1720.
8. Acott TS, Kelley MJ (2008) Extracellular matrix in the trabecular meshwork. *Exp Eye Res* 86(4):543–561.
9. Liton PB, Gonzalez P, Epstein DL (2009) The role of proteolytic cellular systems in trabecular meshwork homeostasis. *Exp Eye Res* 88(4):724–728.
10. Tamm ER (2009) The trabecular meshwork outflow pathways: Structural and functional aspects. *Exp Eye Res* 88(4):648–655.
11. Last JA, et al. (2011) Elastic modulus determination of normal and glaucomatous human trabecular meshwork. *Invest Ophthalmol Vis Sci* 52(5):2147–2152.
12. Grierson I, Rahi AH (1979) Microfilaments in the cells of the human trabecular meshwork. *Br J Ophthalmol* 63(1):3–8.
13. Lütjen-Drecoll E, Futa R, Rohen JW (1981) Ultrahistochemical studies on tangential sections of the trabecular meshwork in normal and glaucomatous eyes. *Invest Ophthalmol Vis Sci* 21(4):563–573.

14. Tektas OY, Lütjen-Drecoll E (2009) Structural changes of the trabecular meshwork in different kinds of glaucoma. *Exp Eye Res* 88(4):769–775.
15. Grierson I, Hogg P (1995) The proliferative and migratory activities of trabecular meshwork cells. *Prog Retin Eye Res* 15(1):33–67.
16. Rodrigues MM, Spaeth GL, Sivalingam E, Weinreb S (1976) Histopathology of 150 trabeculectomy specimens in glaucoma. *Trans Ophthalmol Soc U K* 96(2):245–255.
17. Alvarado J, Murphy C, Juster R (1984) Trabecular meshwork cellularity in primary open-angle glaucoma and nonglaucomatous normals. *Ophthalmology* 91(6):564–579.
18. Gottanka J, Johnson DH, Grehn F, Lütjen-Drecoll E (2006) Histologic findings in pigment dispersion syndrome and pigmentary glaucoma. *J Glaucoma* 15(2):142–151.
19. Alexander RA, Grierson I (1989) Morphological effects of argon laser trabeculoplasty upon the glaucomatous human meshwork. *Eye (Lond)* 3(Pt 6):719–726.
20. Van Buskirk EM (1989) Pathophysiology of laser trabeculoplasty. *Surv Ophthalmol* 33(4):264–272.
21. Acott TS, et al. (1989) Trabecular repopulation by anterior trabecular meshwork cells after laser trabeculoplasty. *Am J Ophthalmol* 107(1):1–6.
22. Dueker DK, Norberg M, Johnson DH, Tschumper RC, Feeney-Burns L (1990) Stimulation of cell division by argon and Nd:YAG laser trabeculoplasty in cynomolgus monkeys. *Invest Ophthalmol Vis Sci* 31(1):115–124.
23. Ding QJ, et al. (2014) Induction of trabecular meshwork cells from induced pluripotent stem cells. *Invest Ophthalmol Vis Sci* 55(11):7065–7072.
24. Zode GS, et al. (2011) Reduction of ER stress via a chemical chaperone prevents disease phenotypes in a mouse model of primary open angle glaucoma. *J Clin Invest* 121(9): 3542–3553.
25. Beckel JM, et al. (2014) Mechanosensitive release of adenosine 5′-triphosphate through pannexin channels and mechanosensitive upregulation of pannexin channels in optic nerve head astrocytes: A mechanism for purinergic involvement in chronic strain. *Glia* 62(9):1486–1501.
26. Clark AF, et al. (1994) Glucocorticoid-induced formation of cross-linked actin networks in cultured human trabecular meshwork cells. *Invest Ophthalmol Vis Sci* 35(1): 281–294.
27. Mao W, Liu Y, Wordinger RJ, Clark AF (2013) A magnetic bead-based method for mouse trabecular meshwork cell isolation. *Invest Ophthalmol Vis Sci* 54(5):3600–3606.
28. Millar JC, Phan TN, Pang IH, Clark AF (2015) Strain and age effects on aqueous humor dynamics in the mouse. *Invest Ophthalmol Vis Sci* 56(10):5764–5776.
29. Ding QJ, Cook AC, Dumitrescu AV, Kuehn MH (2012) Lack of immunoglobulins does not prevent C1q binding to RGC and does not alter the progression of experimental glaucoma. *Invest Ophthalmol Vis Sci* 53(10):6370–6377.
30. Gramlich OW, et al. (2015) Adoptive transfer of immune cells from glaucomatous mice provokes retinal ganglion cell loss in recipients. *Acta Neuropathol Commun* 3:56.
31. Harper MM, et al. (2011) Transplantation of BDNF-secreting mesenchymal stem cells provides neuroprotection in chronically hypertensive rat eyes. *Invest Ophthalmol Vis Sci* 52(7):4506–4515.
32. Kuehn MH, Kim CY, Jiang B, Dumitrescu AV, Kwon YH (2008) Disruption of the complement cascade delays retinal ganglion cell death following retinal ischemia-reperfusion. *Exp Eye Res* 87(2):89–95.
33. Kuehn MH, et al. (2006) Retinal synthesis and deposition of complement components induced by ocular hypertension. *Exp Eye Res* 83(3):620–628.
34. Quigley HA, et al. (2011) Lack of neuroprotection against experimental glaucoma in c-Jun N-terminal kinase 3 knockout mice. *Exp Eye Res* 92(4):299–305.
35. Joe MK, et al. (2003) Accumulation of mutant myocilins in ER leads to ER stress and potential cytotoxicity in human trabecular meshwork cells. *Biochem Biophys Res Commun* 312(3):592–600.
36. Joe MK, Tomarev SI (2010) Expression of myocilin mutants sensitizes cells to oxidative stress-induced apoptosis: Implication for glaucoma pathogenesis. *Am J Pathol* 176(6): 2880–2890.
37. Vollrath D, Liu Y (2006) Temperature sensitive secretion of mutant myocilins. *Exp Eye Res* 82(6):1030–1036.
38. Mi H, Muruganujan A, Casagrande JT, Thomas PD (2013) Large-scale gene function analysis with the PANTHER classification system. *Nat Protoc* 8(8):1551–1566.
39. Kelley MJ, et al. (2009) Stem cells in the trabecular meshwork: Present and future promises. *Exp Eye Res* 88(4):747–751.
40. Du Y, et al. (2012) Multipotent stem cells from trabecular meshwork become phagocytic TM cells. *Invest Ophthalmol Vis Sci* 53(3):1566–1575.
41. Du Y, Yun H, Yang E, Schuman JS (2013) Stem cells from trabecular meshwork home to TM tissue in vivo. *Invest Ophthalmol Vis Sci* 54(2):1450–1459.
42. Abu-Hassan DW, Li X, Ryan EI, Acott TS, Kelley MJ (2015) Induced pluripotent stem cells restore function in a human cell loss model of open-angle glaucoma. *Stem Cells* 33(3):751–761.
43. Mao M, Hedberg-Buenz A, Koehn D, John SW, Anderson MG (2011) Anterior segment dysgenesis and early-onset glaucoma in nee mice with mutation of Sh3pxd2b. *Invest Ophthalmol Vis Sci* 52(5):2679–2688.
44. Kalluri R, Zeisberg M (2006) Fibroblasts in cancer. *Nat Rev Cancer* 6(5):392–401.
45. Wordinger RJ, et al. (1998) Cultured human trabecular meshwork cells express functional growth factor receptors. *Invest Ophthalmol Vis Sci* 39(9):1575–1589.
46. Hematti P (2012) Mesenchymal stromal cells and fibroblasts: A case of mistaken identity? *Cytotherapy* 14(5):516–521.
47. Roubeix C, et al. (2015) Intraocular pressure reduction and neuroprotection conferred by bone marrow-derived mesenchymal stem cells in an animal model of glaucoma. *Stem Cell Res Ther* 6:177.
48. Braunger BM, et al. (2014) Identification of adult stem cells in Schwalbe's line region of the primate eye. *Invest Ophthalmol Vis Sci* 55(11):7499–7507.
49. Tucker BA, Anfinson KR, Mullins RF, Stone EM, Young MJ (2013) Use of a synthetic xeno-free culture substrate for induced pluripotent stem cell induction and retinal differentiation. *Stem Cells Transl Med* 2(1):16–24.
50. Tucker BA, et al. (2011) Transplantation of adult mouse iPS cell-derived photoreceptor precursors restores retinal structure and function in degenerative mice. *PLoS One* 6(4):e18992.
51. Stamer WD, Seftor RE, Williams SK, Samaha HA, Snyder RW (1995) Isolation and culture of human trabecular meshwork cells by extracellular matrix digestion. *Curr Eye Res* 14(7):611–617.
52. Kim CY, Kuehn MH, Anderson MG, Kwon YH (2007) Intraocular pressure measurement in mice: A comparison between Goldmann and rebound tonometry. *Eye (Lond)* 21(9):1202–1209.
53. Boussommier-Calleja A, et al. (2012) Pharmacologic manipulation of conventional outflow facility in ex vivo mouse eyes. *Invest Ophthalmol Vis Sci* 53(9):5838–5845.
54. Camras LJ, et al. (2010) Duration of anesthesia affects intraocular pressure, but not outflow facility in mice. *Curr Eye Res* 35(9):819–827.
55. Ko MK, Yelenskiy A, Gonzalez JM, Jr, Tan JC (2014) Feedback-controlled constant-pressure anterior chamber perfusion in live mice. *Mol Vis* 20:163–170.
56. Trimarchi JM, et al. (2007) Molecular heterogeneity of developing retinal ganglion and amacrine cells revealed through single cell gene expression profiling. *J Comp Neurol* 502(6):1047–1065.
57. Committee on Care and Use of Laboratory Animals (1996) *Guide for the Care and Use of Laboratory Animals* (National Institutes of Health, Bethesda, MD), DHHS Publ No (NIH) 85-23.